

Article

Plasma-Induced Hemi-Wicking on Sanded Polymer Surfaces

Po-Hsien Chiu , Ching-Jung Wu, Chun-Ping Hsiao , Chih-Tung Liu, Mu-Chien Wu and Jong-Shinn Wu *

Department of Mechanical Engineering, National Yang Ming Chiao Tung University, Hsinchu 30010, Taiwan; p.c@nycu.edu.tw (P.-H.C.); wuchingjung@nctu.edu.tw (C.-J.W.); pandarugby@nctu.edu.tw (C.-P.H.); chihlungliu@nctu.edu.tw (C.-T.L.); bwayne.me03g@g2.nctu.edu.tw (M.-C.W.)

* Correspondence: chongsin@faculty.nctu.edu.tw

Abstract: In this paper, a plasma-induced hemi-wicking phenomenon observed on hydrophobic sanded polymer surfaces, polypropylene (PP), polyethylene terephthalate (PET) and polyethylene (PE) is reported. An atmospheric-pressure argon plasma jet was used to treat a limited area of the carefully sanded polymer surfaces to induce the hemi-wicking phenomenon. Such hemi-wicking triggered by the plasma activation is different from the traditional type, which is achieved purely by the surface topography. Surface analyses by X-ray photoelectron spectroscopy (XPS) and water contact analysis (WCA) show that the combination of sanding and plasma treatment increased the oxygen-to-carbon ratio, which is highly beneficial for surface hydrophilicity. The shear stress tests show that the combination of sanding and plasma treatment can enhance the shear stress by 125%, 95%, and 296% on PP, PET, and PE, respectively. The study shows that the newly developed technique by combining the sanding and plasma processing for polymers could be a potentially useful method in future industry applications.

Keywords: hemi-wicking; superwetting; polymer; polypropylene (PP); polyethylene (PE); polyethylene terephthalate (PET); water contact angle (WCA); atmospheric-pressure plasma jet (APPJ); X-ray photoelectron spectroscopy (XPS); sanding; adhesion



Citation: Chiu, P.-H.; Wu, C.-J.; Hsiao, C.-P.; Liu, C.-T.; Wu, M.-C.; Wu, J.-S. Plasma-Induced Hemi-Wicking on Sanded Polymer Surfaces. *Coatings* **2021**, *11*, 871. <https://doi.org/10.3390/coatings11080871>

Academic Editor: Alessandro Patelli

Received: 7 June 2021

Accepted: 18 July 2021

Published: 21 July 2021

Publisher's Note: MDPI stays neutral with regard to jurisdictional claims in published maps and institutional affiliations.



Copyright: © 2021 by the authors. Licensee MDPI, Basel, Switzerland. This article is an open access article distributed under the terms and conditions of the Creative Commons Attribution (CC BY) license (<https://creativecommons.org/licenses/by/4.0/>).

1. Introduction

Polymers are often utilized in packaging, vehicles, clothing, and agriculture, among others, and have many good merits including light weight, easily shaped and low processing costs [1]. Adhesion of polymer is important in many industries, for example, the semiconductor industry which requires better adhesion between the encapsulant, lead frame and the silicon chip to improve reliability, resistance to package cracking, and movement resulting from the thermal stresses [2,3]. However, polymers exhibit hydrophobic characteristics with poor wettability, and detachment occurs because of the difference of surface free energy in the interface between two polymers [4]. Thus, an efficient and cost-effective surface modification is essential for polymers.

Sanding can increase the contact area between the adhesive and the surface, and thus the adhesive strength. The process for sanding the bonding surfaces of the adherends is clearly stated as one of the required physical treatments including acids, bases and flames for modifying the surfaces before adhesive bonding or coating in the industrial standard [5]. Among these methods, sanding with either fine-grit sandpaper or emery cloth is the most common way to modify the surface. However, sanding disadvantageously develops continuous rough microstructures on the surface, and dramatically decreases the surface hydrophilicity [6]. Thus, to maintain the advantage of large contact area of the sanding technique but increase the hydrophilicity of the surface at the same time is critical in the polymer surface treatment.

Plasma activation has been considered as one powerful technique for surface modification including flaming, chemical etching and solvent degreasing for polymers with a low surface energy which causes poor wettability and negatively affects adhesive bonding and

coating [7–10]. Among varieties of plasma activation, the low-pressure nonequilibrium plasma technology has been applied to modify surface properties [1,11]. However, reliable sealing of the chamber and expensive vacuum equipment are required which makes it difficult to integrate into normal production lines, and thus the application feasibility is limited. On the contrary, the atmospheric-pressure plasma jet (APPJ) are free of these disadvantages and proved effective on the polymer for adhesive bonding [12–15]. Because APPJ can be applied at an ambient pressure, APPJ does not require equipment including vacuum chambers, load locks and vacuum pumps, and can be easily integrated into production lines that include, for example, adhesive dispensing or powder spray [13]. Plasma treatment on polymeric surfaces involves the interaction of free radicals and ions with the treated specimen. Such interaction modifies the surface chemical structure and morphology of polymeric materials, and improves the wettability [13,14]. For example, Chiang et al. revealed that, for the PP films, the contact angle (CA) decreases dramatically from 103° to less than 30° after being treated by an APPJ under atmospheric-pressure conditions [16].

Hemi-wicking refers to the behavior when liquid wicks into the gaps inside a texture when a droplet is falling on micro-textured hydrophilic surfaces [17,18]. Quéré described that the liquid wets the inside of the texture but not the top of the texture [19]. In other words, hemi-wicking is the spreading of a liquid driven by capillarity on a rough hydrophilic surface and results in superwetting [20,21]. Hemi-wicking has many important potential applications in inking, printing, boiling heat transfer and condensation, to name a few [21]. For example, the morphologically-driven hemi-wicking was utilized for the enhancement of boiling heat transfer performance of the convective heat dissipation capacity of critical heat flux [22]. Furthermore, the hemi-wicking also made condensate spread quickly [23]. Currently, the studies related to hemi-wicking mainly focus on the surface topography [17,21,23]. Since plasma can be easily used to modify the surface properties of many kinds of polymer surfaces as described earlier, we wonder if the combination of the surface topology manipulation (mechanical effect) with plasma activation (chemical effect) can be a new alternative of controlling the hemi-wicking phenomenon for polymers.

To sum up, sanding is widely used to increase surface contact area, and the plasma activation has the great potential to enhance the wettability, but the effect achieved by the combination of them is rarely explored. In this study, we applied APPJ to treat the sanded polymer surfaces to improve the surface wettability and adhesion of the polymers. With understanding of more detailed underlying mechanism, we would like to take advantage of both methods to achieve the hemi-wicking phenomenon and form superwetting on different kinds of polymer surfaces.

The remainder of this paper is organized as follows: the Experimental Methods are introduced next, followed by the Results and Discussion, which includes characterization of the electrical properties of APPJ, optical emission spectroscopy (OES) data, snapshots of hemi-wicking, CA measurements, XPS analysis and shear stress measurements. Finally, some major findings of this paper are summarized.

2. Materials and Methods

2.1. APPJ System Configuration and Instrumentation

Figure 1a shows the schematic diagram of an APPJ system, including a patented APPJ device along with the instruments used for the measurements of electrical properties. Only argon was used as the working gas in this study, although the APPJ device is capable of using gases including helium, argon, nitrogen and oxygen for generating the gas discharge jet [24]. Figure 1b illustrates the design of the patented APPJ device including a quartz tube with an inner diameter of 6 mm and outer diameter of 8 mm, acted as a dielectric layer. A stainless-steel rod was placed inside the quartz tube to act as a power electrode. The rod was 45 mm in length and 6 mm in diameter. The rod had six longitudinal grooved channels on the surface to allow the working gas passing with a larger electric field when the power source was applied. The bottom edge of the power electrode was positioned 5 mm above the end of the quartz tube. An aluminum foil was wrapped around outside

the quartz tube as the ground electrode. The quartz tube along with the rod was mounted in a chamber made of 3D-printed ABS material containing electric lines and a gas input. The argon gas (99.99%) with impurities (oxygen and water at a level of tens of and several ppm, respectively) flows from the gas bottle to the quartz tube of the APPJ device. The APPJ device was driven by an in-house sinusoidal power supply (0–20 kV peak-to-peak, 20–25 kHz, 60 W maximum power output, 10 cm × 10 cm × 20 cm in size). Figure 1c shows a typical image of the argon discharge.

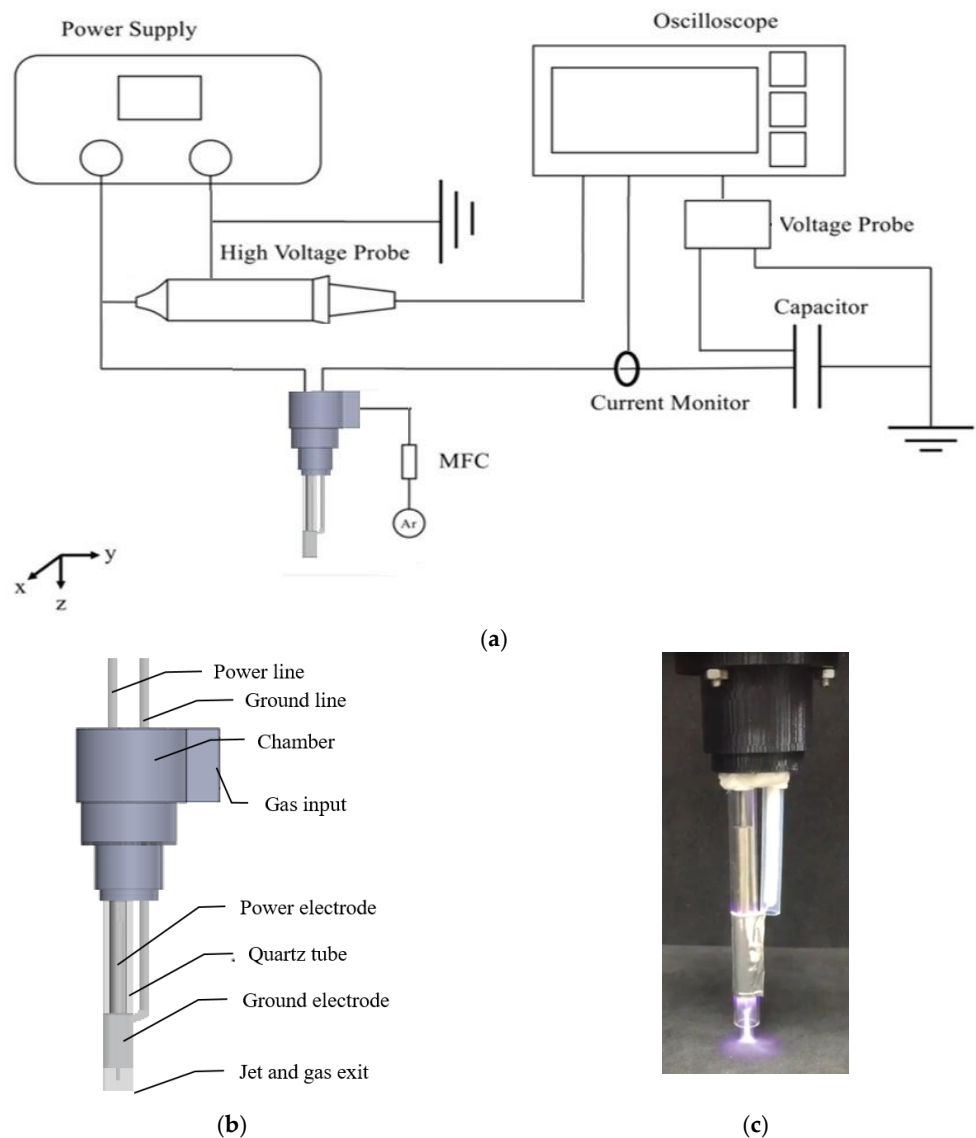


Figure 1. (a) Schematic of system including an APPJ device and electrical measurement devices; (b) schematic of the APPJ device; and (c) snapshot of the APPJ device with the generated plasma jet.

The applied voltage and current signals were measured by a high-voltage probe (Tektronix P6015A, Tektronix Inc., Beaverton, OG, USA) and a Rogowski coil (IPC CM-100-MG, Ion Physics Corporation Inc., Fremont, NH, USA), respectively, through a digital oscilloscope (Wavesurfer 3054, Teledyne Technologies Incorporated, Thousand Oaks, CA, USA). To measure the plasma absorbing power, a 4.7 nF capacitor was placed between the ground electrode and the ground. The voltage across the capacitor was measured using a differential probe (ADP1025, Acute Technology Inc., New Taipei, Taiwan). The waveforms of voltage and current both on the power electrode and across the capacitor

were recorded by the oscilloscope. These data were averaged over 20 cycles to reduce the statistical uncertainties. In addition, the optical emission spectral intensity of the APPJ in the post-discharge region was measured using a monochromator and a photomultiplier tube through an optical fiber and lens (Action SP 2500i; Princeton Instruments, Acton, MA, USA). Data were obtained and analyzed with the PlasusSpecLine spectroscopy software (Version 2.13).

2.2. Polymer Surface Treatment Test Conditions

Films of polymers including polypropylene (PP), polyethylene (PE) and polyethylene terephthalate (PET) were used as the test samples. These films were first sanded by a sanding machine (BOSCH GSS1400A, Gerlingen, Germany) with a sandpaper (Kosta Delta, Ampmate Power Tool co., Taichung, Taiwan) of AA 320 grit size (0.21–0.25 μm in Ra and 0.23–0.28 μm in Rms), before the plasma jet treatment. In the cases with the plasma treatment, the surfaces of the films were positioned 5 mm away from the exit of the APPJ, where the plasma jet was impinged directly on the surface of the specimen for various times.

2.3. Surface Properties Characterization

The polymer surfaces before and after the plasma jet treatment were analyzed by X-ray photoelectron spectroscopy (XPS hereafter, ULVAC-PHI PHI 5000 Versaprobe II, ULVAC-PHI, Inc., Kanagawa, Japan) to reveal changes in the chemical composition of the material. The treated specimens were stored in small cells and sent to the XPS facility right after surface preparation, in order to minimize experimental errors due to potential ambient air surface reaction. It took 20 min to transfer the treated samples to the XPS facility, and it took 0–2 h to carry out the XPS analysis for each sample. The specimens were characterized without any sputtering to collect photoelectron spectra of the O1s, N1s and C1s. The X-ray beam generator was operated at 50 W, and the pressure in the analyzing chamber was maintained below 1.3×10^{-7} Pa during the analysis. The analysis beam diameter of the X-ray beam was 200 μm , and spectra were acquired at a detection angle of 45° with respect to the analyzer with 117.40 eV pass energy.

Water contact angles (WCAs) before and after the plasma jet treatment were measured by a commercial KRÜSS Easy Drop optical system (KRÜSS GmbH, Hamburg, Germany). In this paper, distilled water drops of 2 μL were used as the test liquid. In addition, the morphology of the water droplets on the surface was observed using a video camcorder (Nikon D700, Nikon Corporation, Tokyo, Japan) at the same time. The temperatures over the plasma-treated area of the samples were measured by a thermal camera for smartphones (FLIR ONE Pro, FLIR Systems, Inc., Wilsonville, OR, USA) with FLIR VividIR™ image processing.

Variations in surface morphology were evaluated by a scanning electron microscope (SEM hereafter, Phenom ProX, Phenom-World, Eindhoven, The Netherlands). A light gold coating was sputtered on samples by a Cressington sputter coater (Ted Pella, Inc., Redding, CA, USA) to eliminate the charging effect. The electron beam voltage was 5 or 10 kV. The SEM images were captured by magnifying the measurement 4000 times. Atomic force microscopy (AFM) is not listed as the measurement method for the surface morphology in this study because the fragile probe was damaged by the rugged undulation when scanning on the sanded samples.

2.4. Adhesive Stress Measurement

The shear stress of the adhesive bonding was measured to verify the effect on the adhesive bonding based on the industrial standard [25]. Each specimen of a bonding pair is a rectangle with 25.4 mm width and 140 mm length. The hydrophilic adhesive (Scotch 540-30, 3M, Saint Paul, MN, USA), which contains polyvinyl acetate and ethanol, was applied on each specimen in a length of 20 mm from one end. After a pair of specimens were bonded, a digital force gauge (FSH-500N, YOTEC Precision Instrument, Hsinchu,

Taiwan) was used to test the shear stress of the adhesive bonding. The specimens were tested by the load rate in 1 mm/min.

While inspecting the surface of the polymer films, studies have shown the aging characteristics of plasma-treated surfaces [26,27]. Modified surfaces are susceptible to aging effects when exposed to air, and may revert from hydrophilicity to hydrophobicity with time [28–30]. Thus, time is critical for the implementation of this surface preparation technique on the polymer film. In this study, to avoid aging, WCA measurements and the adhesion of the paired samples for shear stress test were performed 2 min after the plasma activation in this study.

3. Results

3.1. APPJ Characterization

Figure 2 shows the typical measured waveforms of applied voltage and discharge current of the argon APPJ, with a gas flow rate of 5 slm driven by a power of 20 W, with a frequency of 20 kHz. The results show that the amplitude of the voltage was about 4.5 kV, and the peak current can reach 25 mA. Figure 3 shows the corresponding Lissajous figure obtained for the same test conditions. The power absorptions of the plasma can be calculated by integrating the applied voltage and charge in the diagram within a cycle, and then dividing by the period of the cycle [31–33]. The calculated absorption power was 6 W, and the efficiency of the APPJ device was 30%, which is defined as the plasma absorbing power divided by the input power of power supply (20 W in this paper).

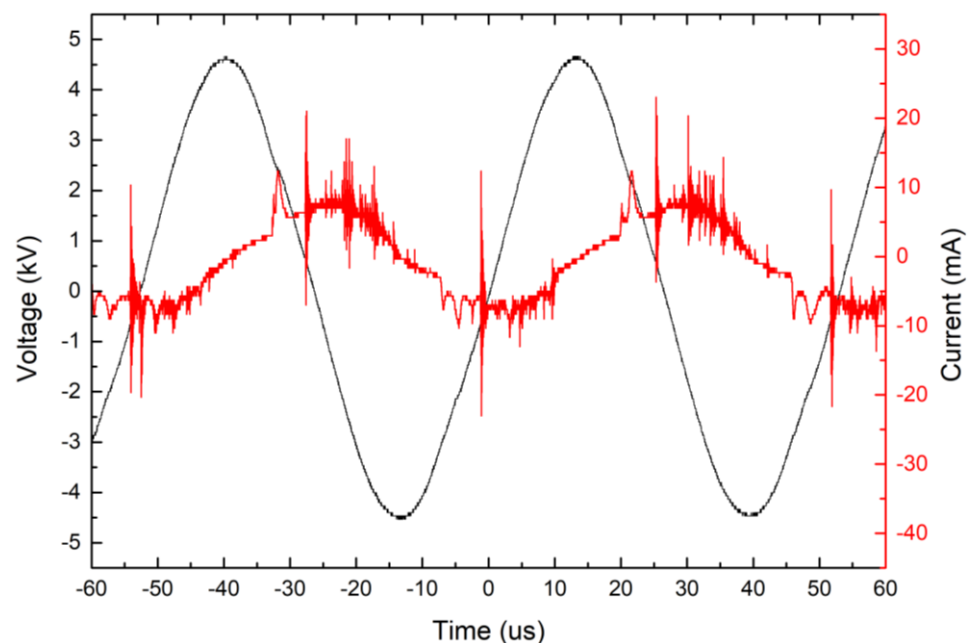


Figure 2. Typical current and voltage waveforms for the APPJ.

Figure 4 shows the OES spectral data of the APPJ at a distance of 5 mm from the jet exit, which is the position of the specimen surface that was treated by the plasma jet. The measured wavelengths were in the UV range (280–400 nm) and visible range (680–880 nm). The OES data show a strong OH* emission at 309 nm and several excited argon emission peaks in the range of 690–850 nm, which was similar to the previous studies [34,35]. The existence of strong OH* is highly beneficial for creating a hydrophilic surface, since it can generate many dangling bonds by reacting with the surface chemical bonds [36–38].

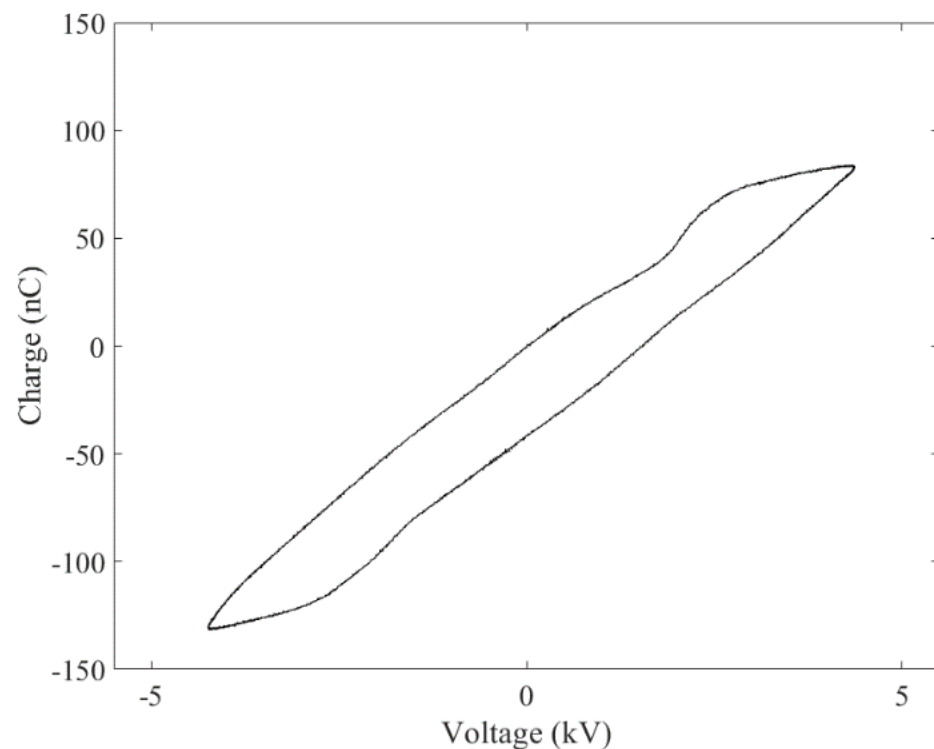
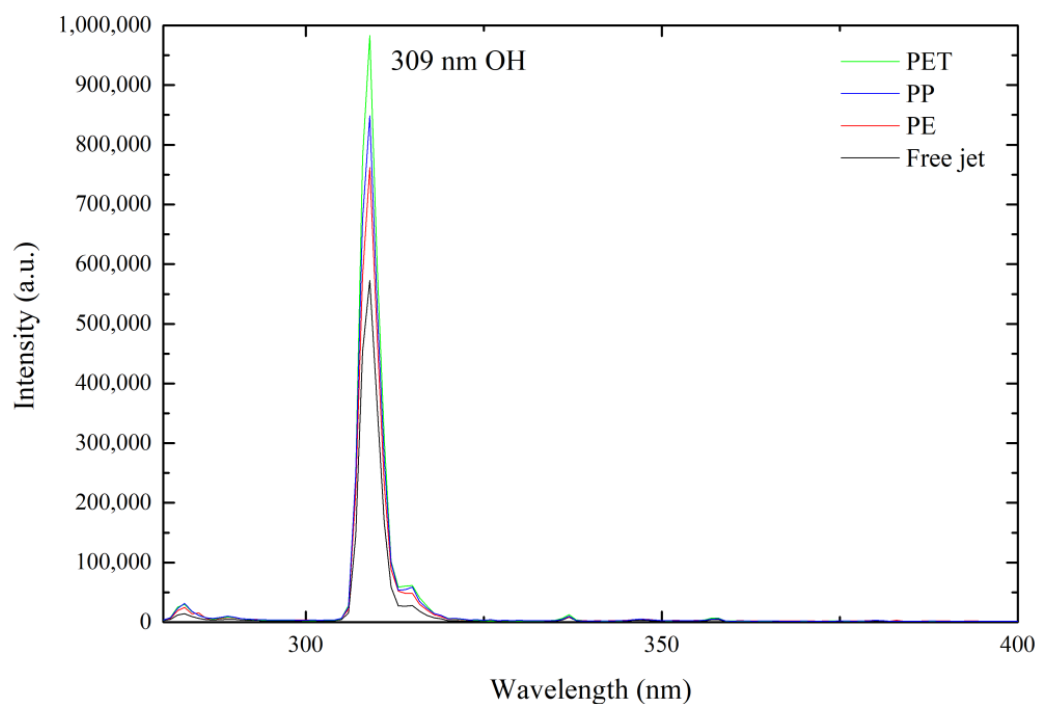


Figure 3. Lissajous diagram of the APPJ.

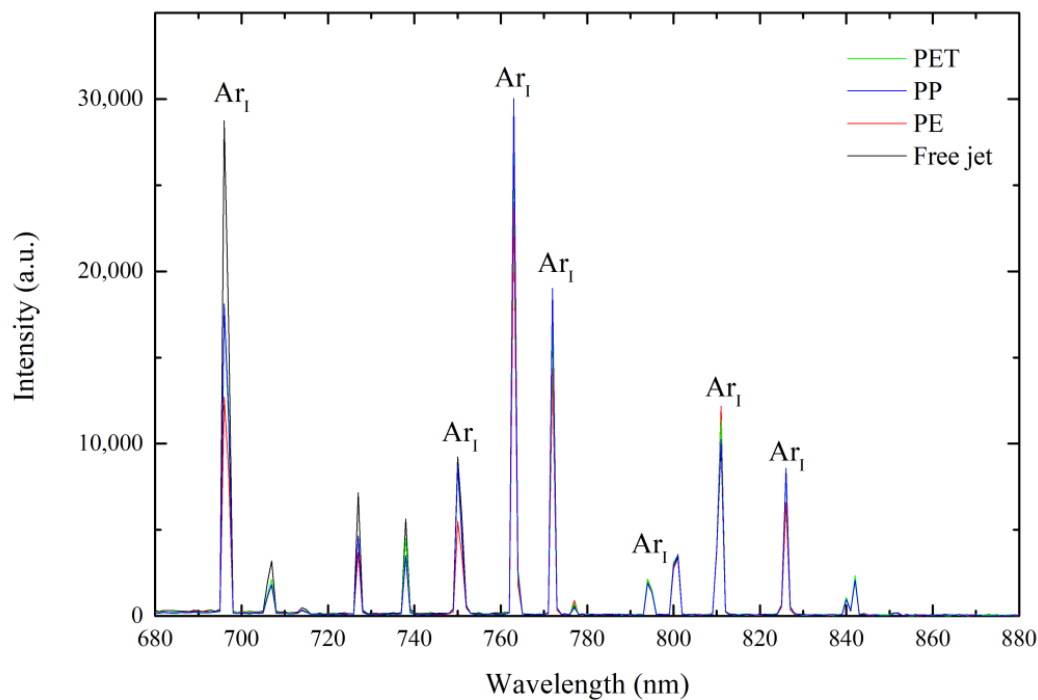
Figure 5 shows the surface temperature measured on the PP surface near the plasma jet after various plasma treatment times. The thermal camera measured similar surface temperatures over treating time distribution for PET and PE. The surface temperatures increased with increasing treatment time but were much lower than the melting temperatures of PP, PET, and PE, which are about 179, 264, and 141 °C respectively.

3.2. Hemi-Wicking

In this study, hemi-wicking was achieved on a polymer surface after it was sanded and then applied with plasma activation. To investigate the hemi-wicking phenomenon, Figure 6a,b shows the snapshots taken from the experiments to demonstrate how a droplet changed on a sanded PP surface after the sanded PP surface was treated by the APPJ for 60 s. Before a Deionization (DI) water droplet was released to fall, a transparent PP film was sanded to be translucent, and a circle was then drawn on the back side of it to avoid any possibility that the ink would affect the water flow on the front side. The blurry image shown in Figure 6a is the circle drawn on the back side of the specimen to indicate the plasma-treated area on the front side. The circle had a diameter of 10 mm and was an approximate area impinged by the APPJ. Then, on the front side of the PP film, the plasma jet was applied on the area inside the circle, while the area outside the circle was left as non-plasma-treated. In the WCA test, a droplet was released to fall inside the circle as shown in Figure 6a, and then seeped very rapidly into the plasma-treated area inside the circle as shown in Figure 6b. Figure 6b shows that the water of the droplet did not stop in the border of the plasma-treated area, but spread to the non-plasma-treated area outside the circle. The mark of the circle became clear and shows that the water had filled the micro-trenches made by the sanding treatment. Similarly, Figure 6c,d shows the hemi-wicking phenomenon on a PET film, and Figure 6e,f shows the hemi-wicking phenomenon on a PE film after being treated with sanding and then APPJ.



(a)



(b)

Figure 4. OES results for the argon-based APPJ in (a) wavelength 280–400 nm; and (b) wavelength 680–880 nm.

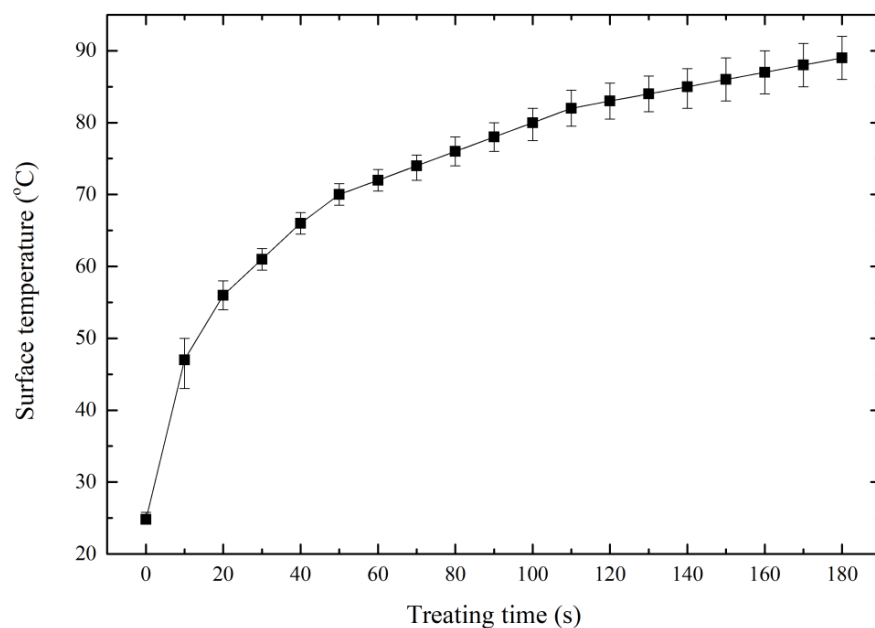


Figure 5. Surface temperature on the PP surface after various plasma treatment times. The thermal camera measured similar surface temperature during treatment time distribution for PET and PE.

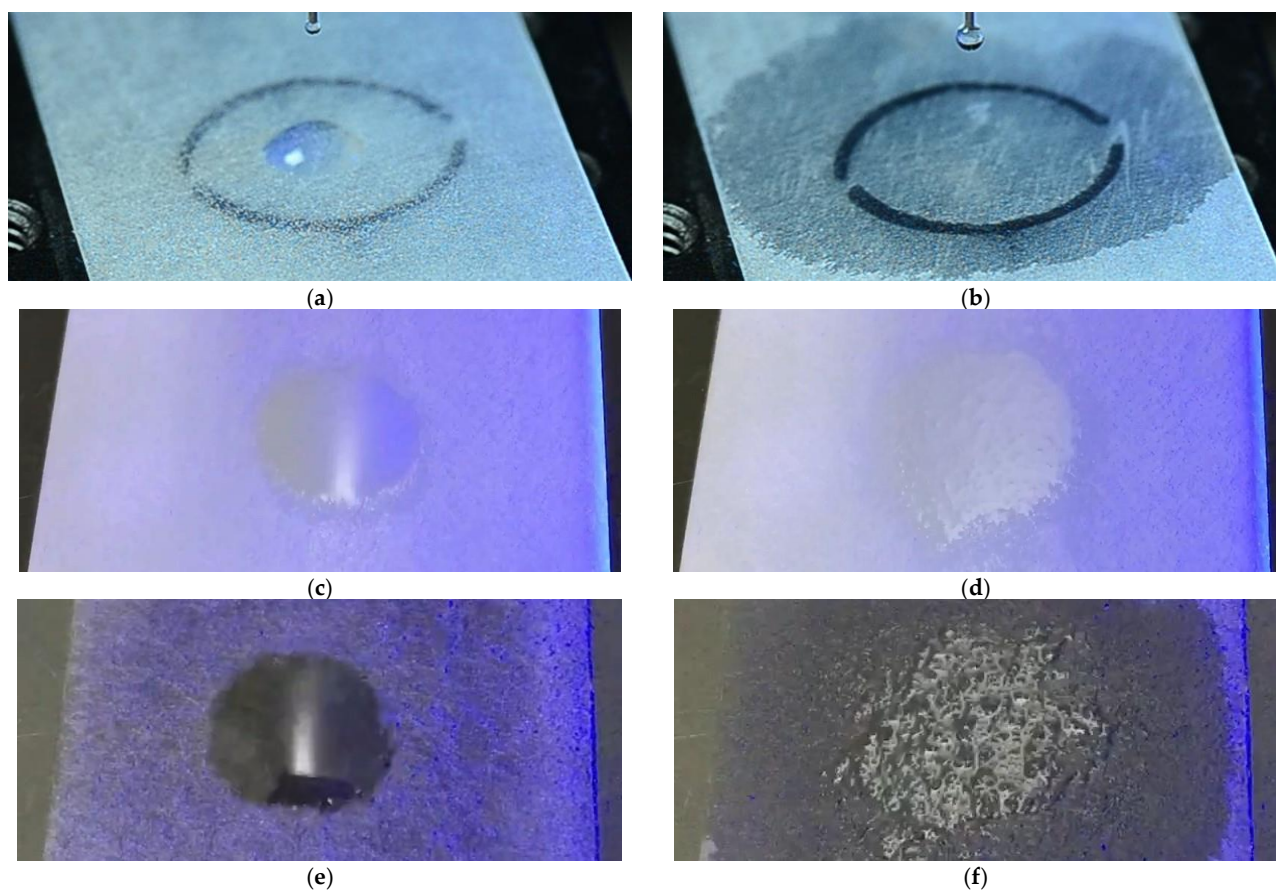


Figure 6. Snapshots for sanded films taken after being treated with APPJ at the moments that (a) a droplet was falling on a PP film initially; (b) the drop was spreading over the PP film; (c) a droplet was falling on a PET film initially; (d) the drop was spreading over the PET film; (e) a droplet was falling on a PE film initially; and (f) the drop was spreading over the PE film.

Figure 7a is typical SEM micrograph of untreated PP surface. Figure 7b,c is the SEM images of the micro-trenches formed on the PP surface by the sanding process, and by the sanding and plasma treatment, respectively. Based on Figure 7b,c, there is no obvious topography change on the sanded PP surface before and after the plasma treatment. Figure 7d illustrates the proposed schematic diagram of the hemi-wicking on the sanded surface treated by the plasma jet, based on the micro-trenches shown in Figure 7c. By referring to Figure 7d, it demonstrates that the water seeped into the plasma-treated area, and then laterally spread into the non-plasma-treated area through the micro-trenches, since the non-plasma-treated area had a hydrophobic surface that prevented water from getting into the micro-trenches. Further, this proves that the micro-trenches of the sanded surface also have a capillary effect if the water can pass through the sanded surface. In other words, for sanded samples without the plasma activation, the hydrophobicity above the micro-trenches stops the droplet from seeping into micro-trenches, although micro-trenches formed on the polymer surface result in a capillary effect. In this study, the plasma treatment can greatly decrease the hydrophobicity above the micro-trenches to make the water of the droplet seep into the micro-trenches. After some water seeps into the micro-trenches, the capillary effect inside the micro-trenches starts to suck the remaining water into the micro-trenches, and results in the hemi-wicking phenomenon as observed in this study. This phenomenon is similar to the hemi-wicking illustrated in Figure 7e, where the top of the spikes remains dry as the imbibition progresses laterally in the direction marked by “dx”, and thus the liquid wets the inside of the texture, i.e., the micro-trenches, rather than the top of the texture [18,19].

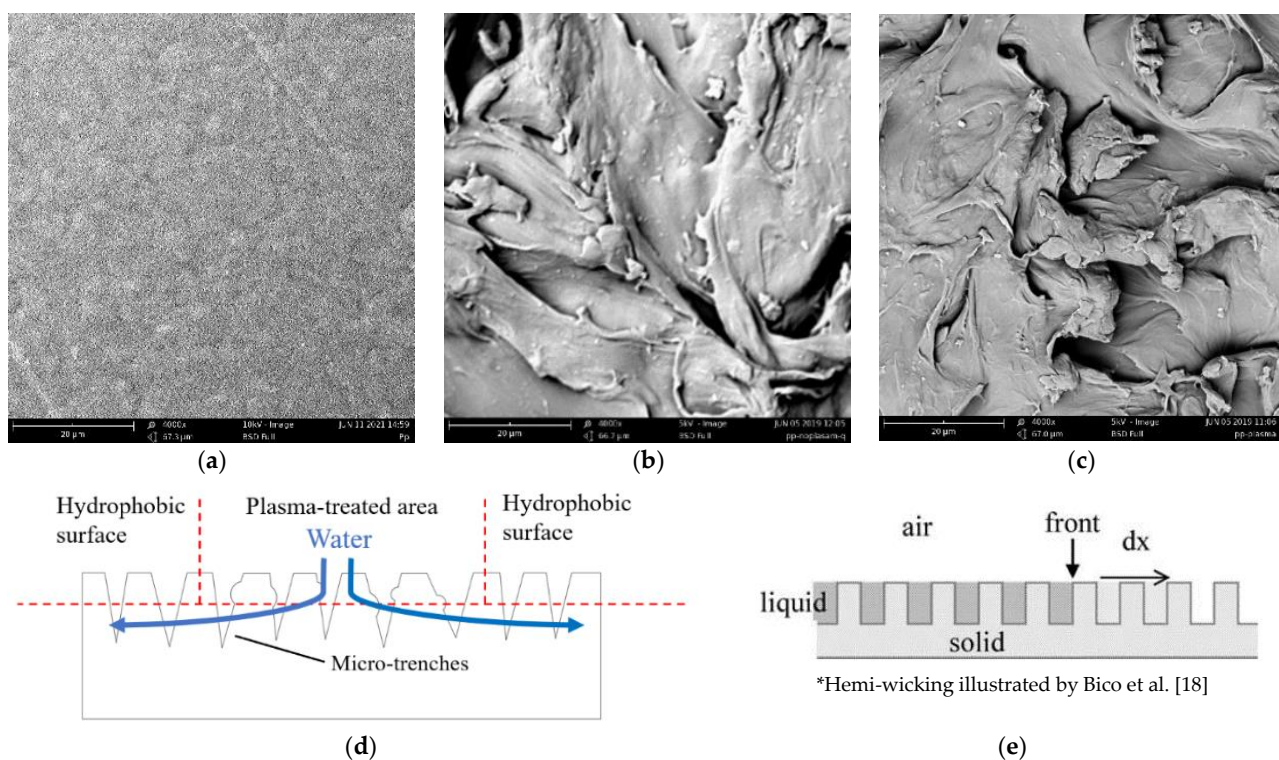


Figure 7. (a) SEM micrograph of untreated PP surface, (b) SEM micrograph of sanded PP surface, (c) SEM micrograph of PP surface treated by sanding and then plasma, (d) diagram of hemi-wicking phenomena on the sanded surface applied by the plasma activation, and (e) diagram of hemi-wicking phenomena illustrated in the prior study.

Indeed, the traditional hemi-wicking can exist forever if the surface topography is not changed. In contrast, the overcoming of the hydrophobic surface can only exist for ten to thirty minutes in the current study. The plasma-induced hemi-wicking in this study disappears after the plasma-treated surface restores its hydrophobicity due to the aging

effect [28,29]. However, the plasma-induced hemi-wicking in this study is much easier to achieve than the morphologically driven hemi-wicking, while the morphologically driven hemi-wicking requires the complicated and expensive construction of the surface topography [17,21,22]. For example, Kim et al. fabricated rough hydrophilic substrates by etching a Si wafer using the deep reactive ion etching process to produce pillar arrays with various geometric parameters [17].

3.3. CA Measurements

The water contact angle measurement is a well-proved method for determining if a surface has been activated, and has been adopted for the testing of hydrophilicity for many polymers and composites [39]. The previous study suggests that the increased wettability (lower WCA) of a specimen surface can increase strength of bonding for the specimen surface [27]. Therefore, a very low WCA, even close to zero, measured at the surface of the polymer film, generally favors the adhesion and coating.

To further elucidate the observed hemi-wicking/superwetting phenomenon, many CA measurements were performed on different kinds of films including PP, PET, and PE after various plasma treating times. Figures 8–10 show the results of the measured WCAs of the PP, PET, and PE films after various plasma treating times. The sanded polymers had higher WCAs than that of the non-sanded polymers before plasma treatment, and both non-sanded and sanded samples had reduced WCAs after plasma treatment. However, the hemi-wicking phenomena was only achieved in the sanded samples where the WCA becomes zero, and never achieved in the non-sanded samples, no matter how long they were treated by the plasma. Although the sanding treatment disadvantageously increases the WCAs of the specimens, it is necessary to achieve the hemi-wicking phenomena.

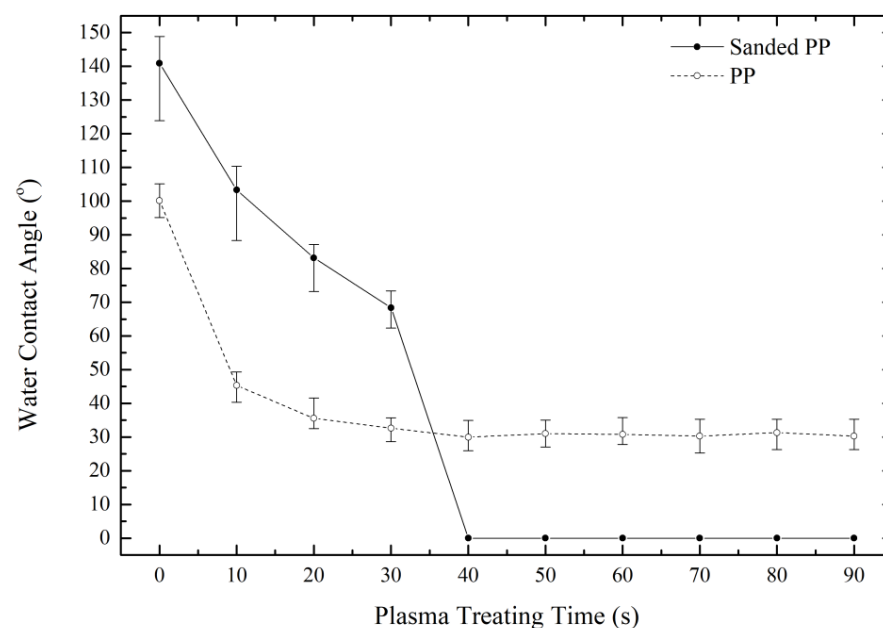


Figure 8. WCAs of PP films after various plasma treating times.

Figure 8 shows the transition timing of the PP films was located between 30 to 40 s of the plasma treating time. At the transition timing, the droplet stayed on the surface of a sanded film for less than a second to more than minutes, before being spread over the sanded film to exhibit the hemi-wicking phenomena. If the plasma treating time exceeded the transition timing, the droplets spread over the sanded films immediately. Similarly, the transition timing of the PET films shown in Figure 9 was located between 50 to 60 s, while the transition timing of the PE films shown in Figure 10 was located between 20 to 30 s. Figures 8–10 show that the longer plasma treating time is required

to achieve the hemi-wicking for a polymer with the higher melting temperature. Such a result matches our prediction, since the polymer with bonds having a higher bond energy requires more plasma treating time to generate dangling bonds for a hydrophilic surface, and there is a positive correlation between the bond energy and the melting temperatures of polymers [40].

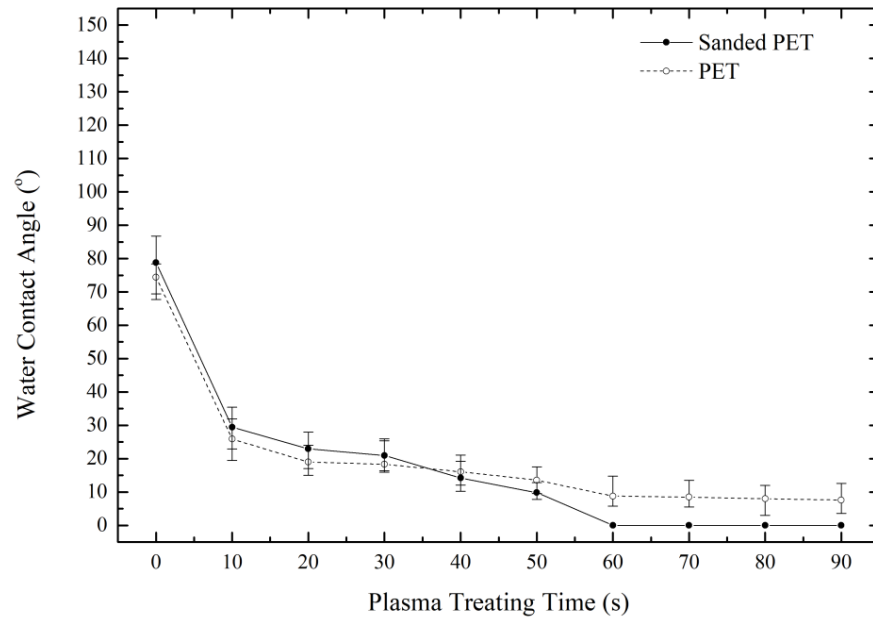


Figure 9. WCAs of PET films after various plasma treating times.

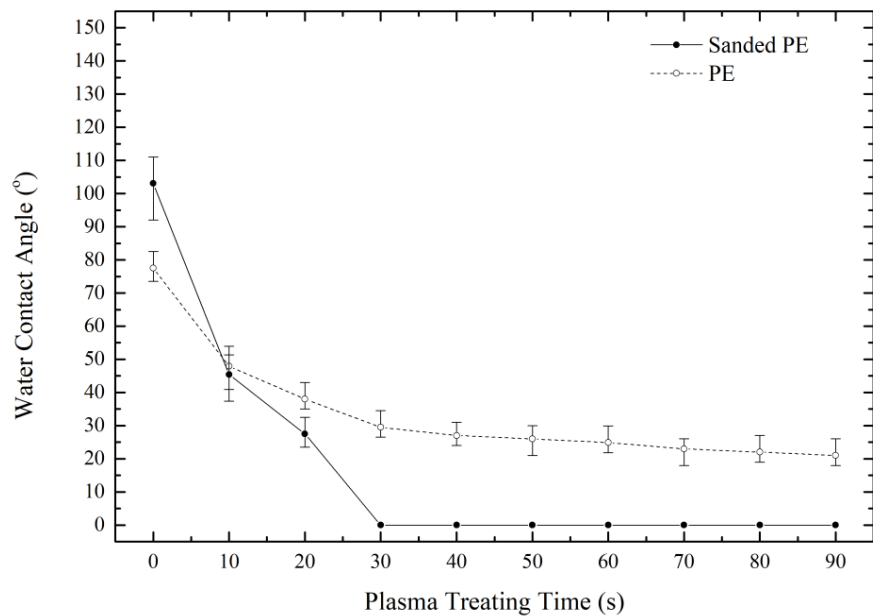


Figure 10. WCAs of PE films after various plasma treating times.

3.4. XPS Analysis

The plasma jet treatment produced radicals or metastable species to impinge the polymer sample and resulted in many active sites on the sampled surface. The active sites on the sample surface were bound to atoms or molecules, e.g., oxygen, in the air [10,41]. XPS analysis can be used to evaluate the chemical composition of the sample surface to investigate the variation of oxygen-containing groups on the sample surface, to identify some factors related to hydrophilicity [42,43]. Thus, XPS measurements were carried out on

polymer films with or without sanding or plasma treatment to understand their influence on the surface modification. Ratios of oxygen-containing groups were calculated by fitting the XPS spectra with Gaussian function based on the C1s peaks of the polymer films.

Figures 11–13 illustrate the C1s spectra of surfaces of the PP, PET, and PE films after different combinations of treatments, including APPJ and sanding. For the cases with the plasma jet activation, the plasma jet impinged perpendicular to the surfaces of the specimens for 60 s. The hemi-wicking phenomena was achieved on the samples treated by both sanding and plasma activation.

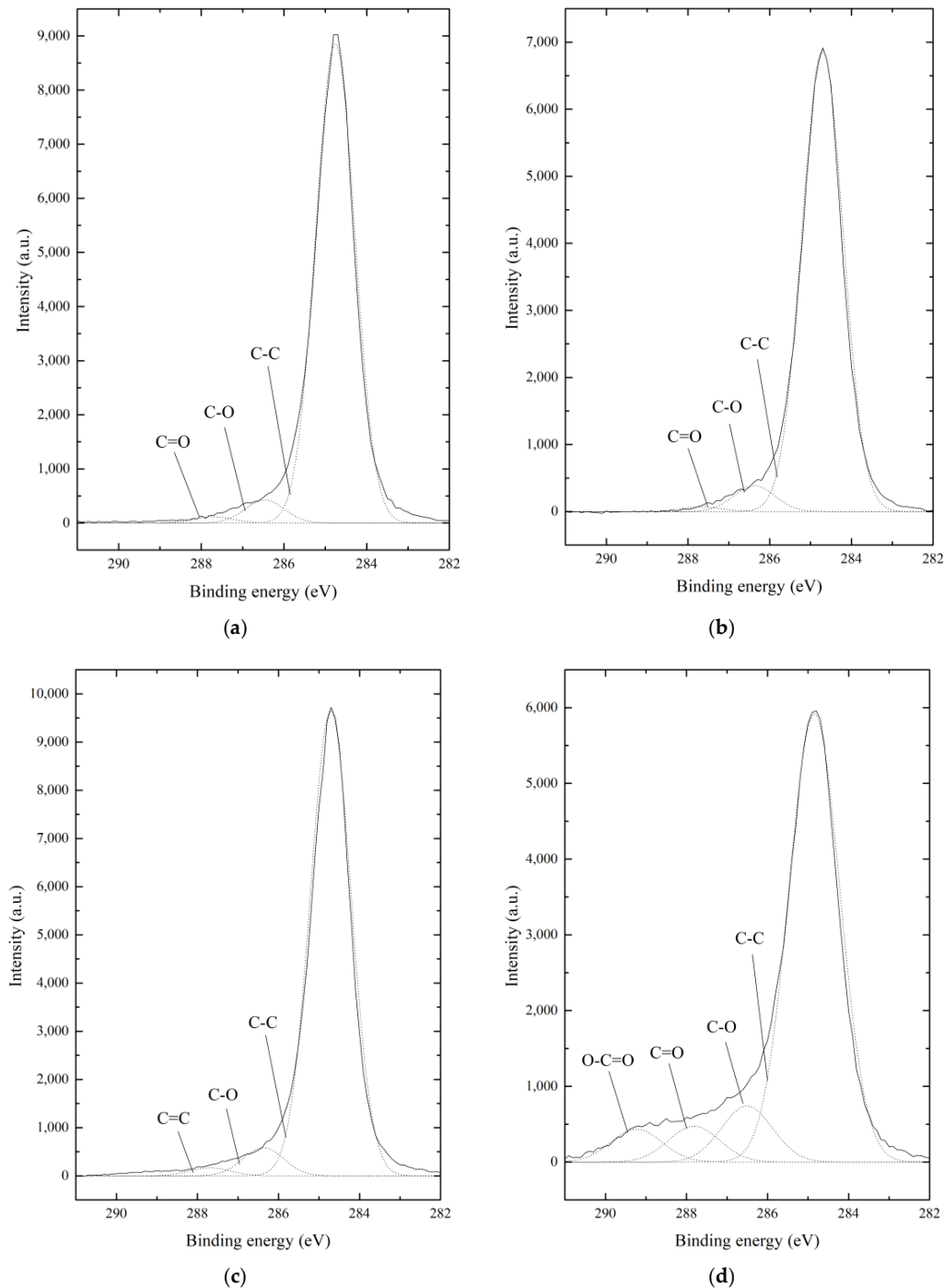


Figure 11. C1s spectra of the PP surface after being treated by (a) none, (b) APPJ only, (c) sanding only, and (d) both sanding and APPJ.

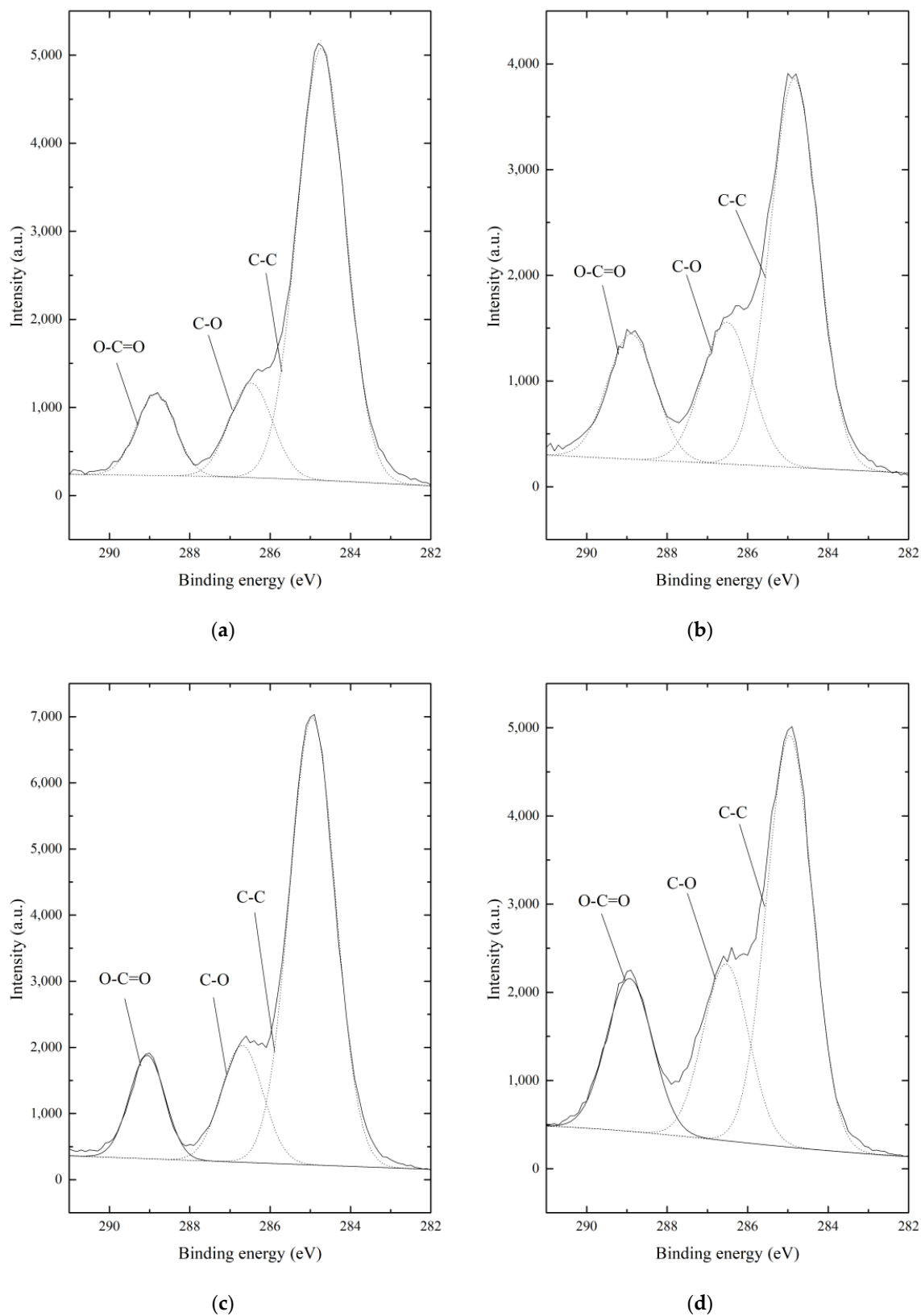


Figure 12. C1s spectra of the PET surface after being treated by (a) none, (b) APPJ only, (c) sanding only, and (d) both sanding and APPJ.

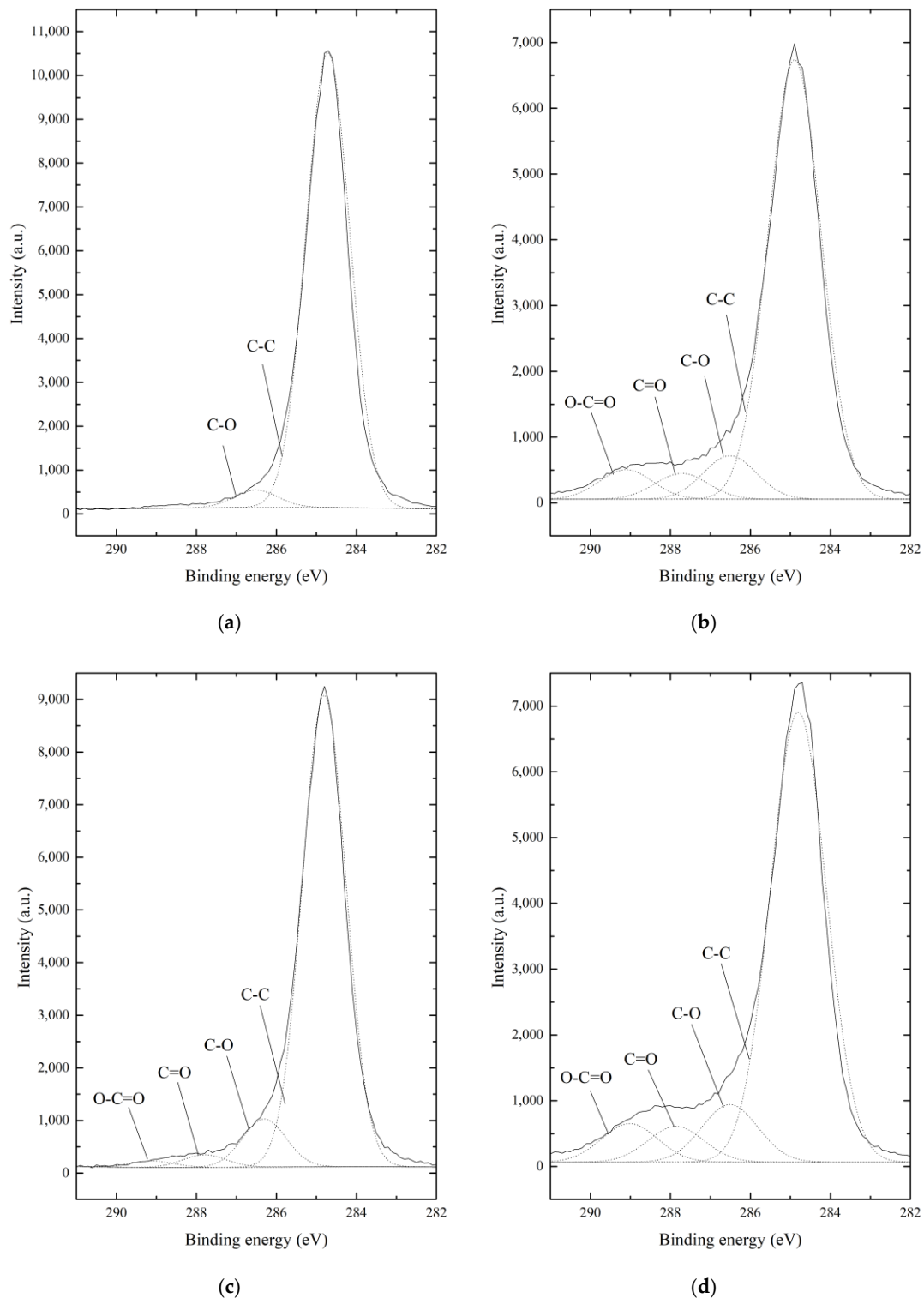


Figure 13. C1s spectra of the PE surface after being treated by (a) none, (b) APPJ only, (c) sanding only, and (d) both sanding and APPJ.

Figure 11a shows that the C1s envelope of the PP films without any treatment was decomposed into three peaks, including a peak at 284.8 eV due to C–C bonds, a peak at 286.5 eV due to C–O functional groups, and a peak at 287.7 eV due to C=O bonds [44]. After both sanding and plasma treatment were applied, the C1s envelope of the PP film was further decomposed into a peak at 289.1 eV attributed to O–C=O groups, and the ratios of C–O, C=O, and O–C=O groups were all increased, as shown in Figure 11d.

Figure 12a shows that the C1s envelope of the PET films without any treatment was decomposed into three peaks, including a peak due to C–C bonds, a peak due to C–O functional groups and a peak attributed to O–C=O groups [45]. Even after both sanding and plasma treatment were applied, the C1s envelope of the PET film was not further decomposed into a peak attributed to C=O groups, but the ratios of C–O and O–C=O groups were both increased, as shown in Figure 12d.

Figure 13a shows that the C1s envelope of the PE films without any treatment was decomposed into two peaks, including a peak due to C–C bonds and a peak due to C–O functional groups [8]. With any sanding or plasma treatment, the C1s envelope was further decomposed into a peak due to C=O bonds and a peak attributed to O–C=O groups, as shown in Figure 13b,d.

In a brief summary, Figures 11–13 illustrate that oxygen atoms involved in C–O bonds were dramatically increased on plasma-treated samples, and PP, PET, and PE films with both sanding and plasma treatments had the highest ratios of C–O and O–C=O groups. Wettability was increased for the increased OH grafting on the surfaces of plasma-treated polymers because more groups with C–O bonds have more OH grafting [36,46].

Table 1 summarizes the measured atomic compositions including carbon, nitrogen, and oxygen, and the fractions of peak area calculated from the XPS spectra of cases illustrated in Figures 11–13. The results show that the plasma activation increased the oxygen to carbon ratio (O/C ratio) dramatically on the surfaces of specimens in both sanded and non-sanded specimens, and also increased the ratio of nitrogen, but in a negligible degree in most cases [44]. The oxygen and nitrogen incorporation were introduced at the reaction between the plasma jet and air which contains oxygen and nitrogen [44]. The results clearly demonstrate that the hydrophilicity increases with increasing O/C ratio of the polymer surface [47–49]. Furthermore, the XPS data shows that any of the PP, PET, and PE films with both sanding and plasma treatment had the highest O/C ratio among the four conditions, including sanding-only and plasma-only treatments. Chiang et al. revealed that O/C ratio increases dramatically for improved hydrophilic surfaces after plasma treatment [17]. Thus, the highly improved surface with the plasma treatment allowed the water droplet to reach the micro-trenches inside the sanded surface, and activated the capillary effect to achieve the hemi-wicking phenomenon.

3.5. Shear Stress Measurements

To demonstrate the effect of the superwetting on the surfaces of specimens, the WCAs and the shear stress of the adhesive bonding between specimens are also included in Table 1. The results obviously show that the superwetting phenomena for the cases with both sanding and plasma treatments results in the highest shear stress of the adhesive bonding between specimens, i.e., 384.4 and 153.7 newtons for the PP and PE films, respectively. This is attributed to the fact that the sanding–plasma cases had the highest O/C ratio and the highest ratios of C–O and O–C=O groups. As for the PET films, Table 1 shows that the highest shear stress was produced by the plasma-only case, but the difference between the sanding–plasma case and the plasma-only case was less than the standard deviation. This is attributed to the fact that the WCA achieved by the plasma-only case was already close to zero, i.e., 8.78° for the PET films, and thus the hydrophilicity improved through the sanding–plasma treatment was limited. Further, the PET films also had the least increase in the O/C ratio and ratios of C–O and O–C=O groups from the plasma-only case to the sanding–plasma case. Regarding the sanding–plasma cases, PP films had higher O/C ratios than PE films, but PP films did not achieve higher shear stress than PE films. Therefore, the comparison of the O/C ratio and ratios of C–O and O–C=O groups can only predict the variation of the shear stress for the same material.

Table 1. Atomic percent concentration and ratio, percent peak area of XPS C1s core level spectra, the corresponded WCA and shear stress results.

No.	Polymer	Treatment	C1s (%)	N1s (%)	O1s (%)	O/C (%)	C-C (%)	C-O (%)	C=O (%)	O-C=O (%)	WCA (°)	Shear Stress (Newtons)
1	PP	–	85.61	0	14.39	16.81	94.21	4.53	1.24	0	100.17	68.2 ± 6.3
2		Plasma	80.16	0	19.84	24.75	93.80	5.24	0.95	0	30.8	133.0 ± 11.2
3		Sanding	89.25	0	10.75	12.04	92.75	5.64	1.61	0	140.88	109.1 ± 9.4
4		Both	68.33	1.73	29.95	43.83	78.21	9.78	6.26	5.74	0	153.7 ± 13.8
5	PET	–	72.15	0	27.85	38.60	74.31	14.39	0	11.30	74.42	169.8 ± 15.2
6		Plasma	63.17	0.93	35.90	56.83	59.03	22.02	0	18.95	8.78	339.8 ± 31.1
7		Sanding	73.37	0	26.63	36.29	70.62	16.73	0	12.65	78.77	259.9 ± 22.4
8		Both	59.57	1.24	39.19	65.79	55.53	23.86	0	20.60	0	331.8 ± 29.9
9	PE	–	88.08	0	11.92	13.53	96.32	3.68	0	0	77.53	97.1 ± 8.7
10		Plasma	71.82	2.18	26.00	36.20	81.61	8.08	4.80	5.51	24.86	263.5 ± 23.5
11		Sanding	81.21	0	18.79	23.13	87.53	8.92	2.35	1.21	103.6	192.1 ± 16.8
12		Both	69.01	3.35	27.64	40.05	77.31	9.91	6.14	6.63	0	384.4 ± 35.1

Measurement of the shear stress was conducted based on ASTM D3163 [25]. Plasma jet activation for 60 s.

Further, the plasma-only treatment produced lower WCAs than the sanding-only treatment, as well as higher shear stress. However, the sanded-only films produced higher WCAs than the controlled films but obtained higher shear stress because sanding increased the contact area between the adhesive and the surface. In brief summary, the sanding process enhanced the adhesive shear stress by 60%, 53%, and 98% on PP, PET, and PE, respectively, as compared to that of the controlled films. Plasma treatment enhanced the bonding shear stress by 95%, 100%, and 171% on PP, PET, and PE, respectively, as compared to that of the controlled films. While combining the sanding process and plasma treatment induces hemi-wicking effect, the shear stress can be enhanced by 125%, 95%, and 296% on PP, PET, and PE, respectively, as compared to that of the controlled films.

4. Discussion

The enhancement of adhesion caused by sanding should be attributed to larger surface contact area, and the enhancement of adhesion caused by plasma treatment should be attributed to surface chemical modification. The combination of the sanding and plasma treatment has both advantages, and further produces plasma-induced hemi-wicking, which achieves the superwetting and has the best performance for enhanced adhesion. Therefore, plasma-induced hemi-wicking on sanded polymers can be a potential technology in future industrial applications.

5. Conclusions

In this work, we have developed a new surface processing technology by applying plasma jet treatment on sanded polymers to achieve the hemi-wicking phenomenon that is highly beneficial for adhesion in practical applications. The combination of the sanding treatment and the plasma activation can achieve superwetting and enhance the shear stress of the adhesive bonding on the sanded and chemical warfare agent (CWA) polymers, to improve adhesion and possibly coating on the hydrophobic surface. Surface XPS analysis and WCA measurements shows that the combination of sanding and plasma treatment increased the O/C ratio, and thus the hydrophilicity of the polymer surfaces. In addition, the results show that the combination can enhance the shear stress more in the range of 95–296%, as compared to the original polymers, if the plasma jet is used for 60 s. Although the sanding–plasma treatment did not achieve an obvious effect on shear stress in the PET films, the sanding–plasma treatment achieved the highest shear stress on the PE and PP films, and thus has the potential to improve the shear stress of other polymers or materials. However, future investigation is required to further clarify the underlying physical and chemical mechanisms that cause this striking phenomenon, and how the aging effect of the plasma-treated surface affects the adhesive bonding strength. Nevertheless,

plasma-induced hemi-wicking found in this study could be a potential technology in future industrial applications.

Author Contributions: P.-H.C. and C.-J.W. performed the experiments and collected the data; C.-P.H., C.-T.L., M.-C.W. and J.-S.W. invented the atmospheric-pressure plasma jet generating device for the experiments; P.-H.C. and J.-S.W. wrote and edited the manuscript. All authors have read and agreed to the published version of the manuscript.

Funding: This research was funded by Ministry of Science and Technology of Taiwan, Grant No. MOST-107-2221-E-009-072-MY3.

Institutional Review Board Statement: Not applicable.

Informed Consent Statement: Not applicable.

Data Availability Statement: Not applicable.

Acknowledgments: The authors would like to thank the Instrumentation Center at National Tsing Hua University and Ching-Wen Tsai for the technical support with the ESCA analysis.

Conflicts of Interest: The authors declare no conflict of interest. The funders had no role in the design of the study; in the collection, analyses, or interpretation of data; in the writing of the manuscript; or in the decision to publish the results.

References

1. Bhowmik, S.; Ghosh, P.K.; Ray, S. Surface Modification of HDPE and PP by Mechanical Polishing and DC Glow Discharge and Their Adhesive Joining to Steel. *J. Appl. Polym. Sci.* **2001**, *80*, 1140–1149. [[CrossRef](#)]
2. Ryntz, R.A. Coating Adhesion to Low Surface Free Energy Substrates. *Prog. Org. Coat.* **1994**, *25*, 73–83. [[CrossRef](#)]
3. Kim, S. The Role of Plastic Package Adhesion in IC Performance. In Proceedings of the 1991 Proceedings 41st Electronic Components & Technology Conference, Atlanta, GA, USA, 11–16 May 1991. [[CrossRef](#)]
4. Żenkiewicz, M. Wettability and Surface Free Energy of Corona-Treated Biaxially-Oriented Polypropylene Film. *J. Adhes. Sci. Technol.* **2001**, *15*, 1769–1785. [[CrossRef](#)]
5. ASTM D2093-03, *Standard Practice for Preparation of Surfaces of Plastics Prior to Adhesive Bonding*; ASTM International: West Conshohocken, PA, USA, 2003. [[CrossRef](#)]
6. Guo, C.; Wang, S.; Liu, H.; Feng, L.; Song, Y.; Jiang, L. Wettability Alteration of Polymer Surfaces Produced by Scraping. *J. Adhes. Sci. Technol.* **2008**, *22*, 395–402. [[CrossRef](#)]
7. Cho, D.L.; Shin, K.H.; Lee, W.-J.; Kim, D.-H. Improvement of Paint Adhesion to a Polypropylene Bumper by Plasma Treatment. *J. Adhes. Sci. Technol.* **2001**, *15*, 653–664. [[CrossRef](#)]
8. Deynse, A.V.; Cools, P.; Leys, C.; Morent, R.; Geyter, N.D. Surface Modification of Polyethylene in an Argon Atmospheric Pressure Plasma Jet. *Surf. Coat. Technol.* **2015**, *276*, 384–390. [[CrossRef](#)]
9. Schulz, U.; Munzert, P.; Kaiser, N. Surface Modification of PMMA by DC Glow Discharge and Microwave Plasma Treatment for the Improvement of Coating Adhesion. *Surf. Coat. Technol.* **2001**, *142–144*, 507–511. [[CrossRef](#)]
10. Lai, J.; Sunderland, B.; Xue, J.; Yan, S.; Zhao, W.; Folkard, M.; Michael, B.D.; Wang, Y. Study on Hydrophilicity of Polymer Surfaces Improved by Plasma Treatment. *Appl. Surf. Sci.* **2006**, *252*, 3375–3379. [[CrossRef](#)]
11. Poncin-Epaillard, F.; Chevet, B.; Brosse, J.-C. Modification of Isotactic Poly (Propylene) with a Nitrogen Plasma; Differences in Comparison to the Treatment with a Carbon Dioxide Plasma. *Makromol. Chem.* **1991**, *192*, 1589–1599. [[CrossRef](#)]
12. Hall, J.R.; Westerdahl, C.A.L.; Devine, A.T.; Bodnar, M.J. Activated Gas Plasma Surface Treatment of Polymers for Adhesive Bonding. *J. Appl. Polym. Sci.* **1969**, *13*, 2085–2096. [[CrossRef](#)]
13. Gonzalez, E.L.; Barankin, M.D.; Guschl, P.C.; Hicks, R.F. Surface Activation of Poly (Methyl Methacrylate) via Remote Atmospheric Pressure Plasma. *Plasma Process Polym.* **2010**, *7*, 482–493. [[CrossRef](#)]
14. Yasuda, H.K.; Sharma, A.K.; Hale, E.B.; James, W.J. Atomic Interfacial Mixing to Create Water Insensitive Adhesion. *J. Adhes.* **1982**, *13*, 269–283. [[CrossRef](#)]
15. Anand, M.; Cohen, R.E.; Baddour, R.F. Surface Modification of Low Density Polyethylene in a Fluorine Gas Plasma. *Polymer* **1981**, *22*, 361–371. [[CrossRef](#)]
16. Chiang, M.-H.; Liao, K.-C.; Lin, I.-M.; Lu, C.-C.; Huang, H.-Y.; Kuo, C.-L.; Wu, J.-S. Modification of Hydrophilic Property of Polypropylene Films by a Parallel-Plate Nitrogen-Based Dielectric Barrier Discharge Jet. *IEEE Trans Plasma Sci.* **2010**, *38*, 1489–1498. [[CrossRef](#)]
17. Kim, J.; Moon, M.-W.; Kim, H.-Y. Dynamics of Hemiwicking. *J. Fluid Mech.* **2016**, *800*, 57–71. [[CrossRef](#)]
18. Bico, J.; Thiele, U.; Quéré, D. Wetting of Textured Surfaces. *Colloids Surf. A Phys. Eng. Asp.* **2002**, *206*, 41–46. [[CrossRef](#)]
19. Quéré, D. Rough Ideas on Wetting. *Physica A* **2002**, *313*, 32–46. [[CrossRef](#)]
20. Spori, D.M.; Drobek, T.; Zürcher, S.; Ochsner, M.; Sprecher, C.; Mühlebach, A.; Spencer, N.D. Beyond the Lotus Effect: Roughness Influences on Wetting over a Wide Surface-Energy Range. *Langmuir* **2008**, *24*, 5411–5417. [[CrossRef](#)]

21. Chen, H.; Zang, H.; Li, X.; Zhao, Y. Toward a Better Understanding of Hemiwicking: A Simple Model to Comprehensive Prediction. *Langmuir* **2019**, *35*, 2854–2864. [[CrossRef](#)]
22. Kim, B.S.; Choi, G.; Shim, D.I.; Kim, K.M.; Cho, H.H. Surface Roughening for Hemi-Wicking and Its Impact on Convective Boiling Heat Transfer. *Int. J. Heat Mass. Transf.* **2016**, *102*, 1100–1107. [[CrossRef](#)]
23. Ghosh, A.; Beaini, S.; Zhang, B.J.; Ganguly, R.; Megaridis, C.M. Enhancing Dropwise Condensation through Bioinspired Wettability Patterning. *Langmuir* **2014**, *30*, 13103–13115. [[CrossRef](#)]
24. Wu, J.-S.; Liu, C.-T.; Hsiao, C.-P.; Wu, M.-C. Atmospheric-Pressure Plasma Jet Generating Device. U.S. Patent 10,121,638, 6 November 2018.
25. ASTM D3163-01, *Standard Test Method for Determining Strength of Adhesively Bonded Rigid Plastic Lap-Shear Joints in Shear by Tension Loading*; ASTM International: West Conshohocken, PA, USA, 2014. [[CrossRef](#)]
26. Morent, R.; Geyter, N.D.; Leys, C.; Gengembre, L.; Payen, E. Study of the Ageing Behaviour of Polymer Films Treated with a Dielectric Barrier Discharge in Air, Helium and Argon at Medium Pressure. *Surf. Coat. Tech.* **2007**, *201*, 7847–7854. [[CrossRef](#)]
27. Hegemann, D.; Brunner, H.; Oehr, C. Plasma Treatment of Polymers for Surface and Adhesion Improvement. *Nucl. Instrum. Methods Phys. Res. B* **2003**, *208*, 281–286. [[CrossRef](#)]
28. Occhiello, E.; Morra, M.; Cinquina, P.; Garbassi, F. Hydrophobic Recovery of Oxygen-Plasma-Treated Polystyrene. *Polymer* **1992**, *33*, 3007–3015. [[CrossRef](#)]
29. Takke, V.; Behary, N.; Perwuelz, A.; Campagne, C. Studies on the Atmospheric Air-Plasma Treatment of PET (Polyethylene Terephthalate) Woven Fabrics: Effect of Process Parameters and of Aging. *J. Appl. Polym. Sci.* **2009**, *114*, 348–357. [[CrossRef](#)]
30. Gotoh, K.; Shohbuke, E.; Kobayashi, Y.; Yamada, H. Wettability Control of PET Surface by Plasma-Induced Polymer Film Deposition and Plasma/UV Oxidation in Ambient Air. *Colloids Surf. A Phys. Eng. Asp.* **2018**, *556*, 1–10. [[CrossRef](#)]
31. Wagner, H.-E.; Brandenburg, R.; Kozlov, K.V.; Sonnenfeld, A.; Michel, P.; Behnke, J.F. The Barrier Discharge: Basic Properties and Applications to Surface Treatment. *Vacuum* **2003**, *71*, 417–436. [[CrossRef](#)]
32. Morent, R.; Geyter, N.D.; Gengembre, L.; Leys, C.; Payen, E.; Vlierberghe, S.V.; Schacht, E. Surface Treatment of a Polypropylene Film with a Nitrogen DBD at Medium Pressure. *Eur. Phys. J. Appl. Phys.* **2008**, *43*, 289–294. [[CrossRef](#)]
33. Wu, M.-C.; Liu, C.-T.; Chiang, C.-Y.; Lin, Y.-J.; Lin, Y.-H.; Chang, Y.-W.; Wu, J.-S. Inactivation Effect of Colletotrichum Gloeosporioides by Long-Lived Chemical Species Using Atmospheric-Pressure Corona Plasma-Activated Water. *IEEE Trans Plasma Sci.* **2019**, *47*, 1100–1104. [[CrossRef](#)]
34. Lin, Z.-H.; Cheng, K.-Y.; Cheng, Y.-P.; Tschang, C.-Y.T.; Chiu, H.-Y.; Yeh, N.-L.; Liao, K.-C.; Gu, B.-R.; Wu, J.-S. Acute Rat Cutaneous Wound Healing for Small and Large Wounds Using Ar/O₂ Atmospheric-Pressure Plasma Jet Treatment. *Plasma Med.* **2017**, *7*, 227–243. [[CrossRef](#)]
35. Cheng, K.-Y.; Lin, Z.-H.; Cheng, Y.-P.; Chiu, H.-Y.; Yeh, N.-L.; Wu, T.-K.; Wu, J.-S. Wound Healing in Streptozotocin-Induced Diabetic Rats Using Atmospheric-Pressure Argon Plasma Jet. *Sci. Rep.* **2018**, *8*. [[CrossRef](#)]
36. Asfardjani, K.; Segui, Y.; Aurelle, Y.; Abidine, N. Effect of Plasma Treatments on Wettability of Polysulfone and Polyetherimide. *J. Appl. Polym. Sci.* **1991**, *43*, 271–281. [[CrossRef](#)]
37. Kamal, S.A.A.; Ritikos, R.; Rahman, S.A. Wetting Behaviour of Carbon Nitride Nanostructures Grown by Plasma Enhanced Chemical Vapour Deposition Technique. *Appl. Surf. Sci.* **2015**, *328*, 146–153. [[CrossRef](#)]
38. Tamada, Y.; Ikada, Y. Cell Adhesion to Plasma-Treated Polymer Surfaces. *Polymer* **1993**, *34*, 2208–2212. [[CrossRef](#)]
39. Williams, T.S.; Yu, H.; Yeh, P.-C.; Yang, J.-M.; Hicks, R.F. Atmospheric Pressure Plasma Effects on the Adhesive Bonding Properties of Stainless Steel and Epoxy Composites. *J. Compos Mater* **2012**, *48*, 219–233. [[CrossRef](#)]
40. Banerjee, S.; Tyagi, A.K. *Functional Materials*; Elsevier: Amsterdam, The Netherlands, 2012. [[CrossRef](#)]
41. Han, S.; Lee, Y.; Kim, H.; Kim, G.; Lee, J.; Yoon, J.-H.; Kim, G. Polymer Surface Modification by Plasma Source Ion Implantation. *Surf. Coat. Technol.* **1997**, *93*, 261–264. [[CrossRef](#)]
42. Liston, E.M.; Martinu, L.; Wertheimer, M.R. Plasma Surface Modification of Polymers for Improved Adhesion: A Critical Review. *J. Adhes. Sci. Technol.* **1993**, *7*, 1091–1127. [[CrossRef](#)]
43. Riccardi, C.; Barni, R.; Selli, E.; Mazzone, G.; Massafra, M.R.; Marcandalli, B.; Poletti, G. Surface Modification of Poly (Ethylene Terephthalate) Fibers Induced by Radio Frequency Air Plasma Treatment. *Appl. Surf. Sci.* **2003**, *211*, 386–397. [[CrossRef](#)]
44. Sarani, A.; Nikiforov, A.Y.; Geyter, N.D.; Morent, R.; Leys, C. Surface Modification of Polypropylene with an Atmospheric Pressure Plasma Jet Sustained in Argon and an Argon/Water Vapour Mixture. *Appl. Surf. Sci.* **2011**, *257*, 8737–8741. [[CrossRef](#)]
45. Fang, Z.; Yang, J.; Liu, Y.; Shao, T.; Zhang, C. Surface Treatment of Polyethylene Terephthalate to Improving Hydrophilicity Using Atmospheric Pressure Plasma Jet. *IEEE Trans Plasma Sci.* **2013**, *41*, 1627–1634. [[CrossRef](#)]
46. Iqbal, M.; Dinh, D.K.; Abbas, Q.; Imran, M.; Sattar, H.; Ahmad, A.U. Controlled Surface Wettability by Plasma Polymer Surface Modification. *Surfaces* **2019**, *2*, 349–371. [[CrossRef](#)]
47. Cui, N.-Y.; Brown, N.M.D. Modification of the Surface Properties of a Polypropylene (PP) Film Using an Air Dielectric Barrier Discharge Plasma. *Appl. Surf. Sci.* **2002**, *189*, 31–38. [[CrossRef](#)]
48. Strobel, M.; Walzak, M.J.; Hill, J.M.; Lin, A.; Karbasheski, E.; Lyons, C.S. A Comparison of Gas-Phase Methods of Modifying Polymer Surfaces. *J. Adhes. Sci. Technol.* **1995**, *9*, 365–383. [[CrossRef](#)]
49. Strobel, M.; Jones, V.; Lyons, C.S.; Ulsh, M.; Kushner, M.J.; Dorai, R.; Branch, M.C. A Comparison of Corona-Treated and Flame-Treated Polypropylene Films. *Plasma Polym.* **2003**, *8*, 61–95. [[CrossRef](#)]